American Mineralogist, Volume 100, pages 824–836, 2015

The origin and implications of clay minerals from Yellowknife Bay, Gale crater, Mars† 🔓

Thomas F. Bristow[1,*], David L. Bish[2], David T. Vaniman[3], Richard V. Morris[4], David F. Blake[1], John P. Grotzinger[5], Elizabeth B. Rampe[4], Joy A. Crisp[6], Cherie N. Achilles[2], Doug W. Ming[4], Bethany L. Ehlmann[5,6], Penelope L. King[7,8], John C. Bridges[9], Jennifer L. Eigenbrode[10], Dawn Y. Sumner[11], Steve J. Chipera[12], John Michael Morookian[6], Allan H. Treiman[13], Shaunna M. Morrison[14], Robert T. Downs[14], Jack D. Farmer[15], David Des Marais[1], Philippe Sarrazin[16], Melissa M. Floyd[10], Michael A. Mischna[6] and Amy C. McAdam[10]

[1]Exobiology Branch, NASA Ames Research Center, Moffett Field, California 94035, U.S.A.
[2]Department of Geological Sciences, Indiana University, 1001 East Tenth Street, Bloomington, Indiana, 47405, U.S.A.
[3]Planetary Science Institute, 1700 E. Fort Lowell, Tucson, Arizona 85719-2395, U.S.A.
[4]ARES Division, NASA Johnson Space Center, Houston, Texas 77058, U.S.A.
[5]Division of Geological and Planetary Sciences, California Institute of Technology, 1200 E. California Boulevard, Pasadena, California 91125, U.S.A.
[6]Jet Propulsion Laboratory, California Institute of Technology, 4800 Oak Grove Drive, Pasadena, California 91109, U.S.A.
[7]Research School of Earth Sciences, Australian National University, Canberra ACT 0200, Australia
[8]Department of Physics, University of Guelph, Guelph, Ontario N1G 2W1, Canada
[9]Space Research Center, University of Leicester, Leicester LE1 7RH, U.K.
[10]NASA Goddard Space Flight Center, Greenbelt, Maryland 20771, U.S.A.
[11]Department of Earth and Planetary Sciences, University of California, Davis, California 95616, U.S.A.
[12]Chesapeake Energy Corporation, 6100 N. Western Avenue, Oklahoma City, Oklahoma 73118, U.S.A.
[13]Lunar and Planetary Institute, 3600 Bay Area Boulevard, Houston, Texas 77058, U.S.A.
[14]Department of Geology, University of Arizona, Tucson, Arizona 85721, U.S.A.
[15]Department of Geological Sciences, Arizona State University, Tempe, Arizona 85281, U.S.A.
[16]SETI Institute, Mountain View, California 94043, U.S.A.

Abstract

The Mars Science Laboratory (MSL) rover Curiosity has documented a section of fluvio-lacustrine strata at Yellowknife Bay (YKB), an embayment on the floor of Gale crater, approximately 500 m east of the Bradbury landing site. X-ray diffraction (XRD) data and evolved gas analysis (EGA) data from the CheMin and SAM instruments show that two powdered mudstone samples (named John Klein and Cumberland) drilled from the Sheepbed member of this succession contain up to ~20 wt% clay minerals. A trioctahedral smectite, likely a ferrian saponite, is the only clay mineral phase detected in these samples. Smectites of the two samples exhibit different 001 spacing under the low partial pressures of H_2O inside the CheMin instrument (relative humidity <1%). Smectite interlayers in John Klein collapsed sometime between clay mineral formation and the time of analysis to a basal spacing of 10 Å, but largely remain open in the Cumberland sample with a basal spacing of ~13.2 Å. Partial intercalation of Cumberland smectites by metal-hydroxyl groups, a common process in certain pedogenic and lacustrine settings on Earth, is our favored explanation for these differences.

The relatively low abundances of olivine and enriched levels of magnetite in the Sheepbed mudstone, when compared with regional basalt compositions derived from orbital data, suggest that clay minerals formed with magnetite in situ via aqueous alteration of olivine. Mass-balance calculations are permissive of such a reaction. Moreover, the Sheepbed mudstone mineral assemblage is consistent with minimal inputs of detrital clay minerals from the crater walls and rim. Early diagenetic fabrics suggest clay mineral formation prior to lithification. Thermodynamic modeling indicates that the production of authigenic magnetite and saponite at surficial temperatures requires a moderate supply of oxidants, allowing circum-neutral pH. The kinetics of olivine alteration suggest the presence of fluids for thousands to hundreds of thousands of years. Mineralogical evidence of the persistence of benign aqueous conditions at YKB for extended periods indicates a potentially habitable environment where life could establish itself. Mediated oxidation of Fe^{2+} in olivine to Fe^{3+} in magnetite, and perhaps in smectites provided a potential energy source for organisms.

Keywords: Mars, Yellowknife Bay, clay minerals, CheMin, XRD, habitability

Introduction

Over the last decade, orbital mineralogical surveys of the surface of Mars have revealed the widespread presence of clay minerals, largely restricted to Noachian age terrains (Poulet et al. 2005; Bibring et al. 2006; Murchie et al. 2009; Ehlmann et al. 2011). As common aqueous alteration products of the basaltic igneous rocks that make up much of the martian crust, these clay minerals may indicate a period in Mars history >3.7 Ga when conditions were wetter and perhaps warmer than today.

* E-mail: thomas.f.bristow@nasa.gov
† 🔓 Open access: Article available to all readers online.

0003-004X/15/0004–824$05.00/DOI: http://dx.doi.org/10.2138/am-2015-5077CCBYNCND

However, questions remain as to whether clay minerals detected from space reflect conditions at or near the surface of Mars or are remnants of subsurface hydrologic systems that were more active early in Mars' history (Ehlmann et al. 2011). Thus establishing the geological context and temporal distribution of clay-bearing deposits has become central to characterizing potential habitable environments for life and the abundance and mobility of water on ancient Mars.

One of the primary science goals of the MSL rover Curiosity is to study a succession of clay mineral- and sulfate-bearing strata near the base of a 5 km thick sequence of layered rocks exposed in the flanks of Aeolis Mons, informally called Mt. Sharp, a mound that rises from the center of ~150 km diameter Gale crater (Anderson and Bell 2010; Milliken et al. 2010). The types of clay minerals and the temporal succession of clay-bearing strata overlain by sulfate-bearing lithologies bear a striking resemblance to posited global mineralogical trends documented from space, which may reflect changes in climate and the availability of water on early Mars (Grotzinger and Milliken 2012).

After an initial commissioning phase, Curiosity drove eastward from Bradbury Landing where it encountered clay mineral-bearing mudstones at Yellowknife Bay (YKB) ~500 m east of the rover's landing site (Vaniman et al. 2014). The mudstones are part of a section of the fluvio-lacustrine YKB formation, derived from erosion of rocks along the Gale crater rim, as confirmed by a bulk K-Ar age of 4.21 ± 0.35 billion years (Farley et al. 2014). However, the stratigraphic relationships between the YKB formation and either the Peace Vallis fan or the strata of lower Mt. Sharp are uncertain. In either case, strata of the YKB formation, including the clay mineral-bearing Sheepbed member, post-date the Noachian-Hesperian boundary and are younger than the majority of clay minerals documented on Mars from orbit (Ehlmann et al. 2011; Vaniman et al. 2014; Grotzinger et al. 2014). The clay minerals at YKB are interpreted to have formed in situ and indicate paleoenvironmental conditions within the fluvio-lacustrine system were potentially habitable for life (Vaniman et al. 2014; Grotzinger et al. 2014). The age of the deposits implies habitable conditions on Mars persisted, at least locally, for longer than previously thought. This paper provides a focused examination of the origins of the clay minerals and associated mineralogical processes, considering their sedimentological/mineralogic context, regional geology, and the geochemical compositions of the host sediments.

Sedimentary context

A ~4.75 m thick succession of flat lying, decimeter-scale sedimentary strata, collectively known as the YKB formation, is exposed in the western margin of YKB—a local depression ~18 m below the elevation of the Bradbury landing site. The base of the YKB formation is not exposed and total thickness is not known. The YKB formation largely consists of basaltic mudstones and sandstones and is informally subdivided into the Sheepbed, Gillespie Lake, and Glenelg members, with the Sheepbed member mudstone the lowest unit exposed (Grotzinger et al. 2014). Members are defined based on differences in lithology, bedding geometry, sedimentary structures, and lateral extent. Facies analysis supports a fluvio-lacustrine origin for these strata (Grotzinger et al. 2014).

The Sheepbed member is of particular scientific interest because evidence points to deposition in a standing body of water (Grotzinger et al. 2014). Regional mapping indicates a minimum deposit extent of 4 km^2, with a thickness of at least 1.5 m at YKB. The Sheepbed mudstone consists of homogenous, fine-grained sediments (nearly all discernable grains <50 μm, with the clay mineral content presumably <2 μm) with a few very thin intercalated beds that resist erosion. Curiosity carried out a detailed geochemical and textural examination of a traverse through the Sheepbed. The mudstone contains early diagenetic features including nodules, hollow nodules and raised ridges (Grotzinger et al. 2014; Stack et al. 2014; Siebach et al. 2014). The ridges tend to be elevated in magnesium relative to the surrounding sediments (Léveillé et al. 2014). The bulk chemistry of rocks throughout the member is similar to average martian crust (McLennan et al. 2014). Together, textures, bulk chemistry, and the sedimentary context of the Sheepbed are most amenable to interpretation as proximal lacustrine deposits (Grotzinger et al. 2014).

The Sheepbed member (and other parts of YKB formation) experienced a period of aqueous alteration post-dating lithification. A network of brittle fractures, up to 8 mm in width and lacking preferred orientation, cut early diagenetic features and are filled with light-toned hydrated and dehydrated sulfates including bassanite and anhydrite (Grotzinger et al. 2014; Vaniman et al. 2014). These Ca-sulfates fill some of the hollow nodules that are intersected by the late-diagenetic fractures.

Curiosity drilled two ~6 cm deep holes in the Sheepbed member at sites named John Klein and Cumberland. The sites are 2.5 m apart and are within ~30 cm of each other stratigraphically. John Klein is a representative lithology of most of the Sheepbed member, whereas Cumberland contains abundant early diagenetic concretions, especially hollow nodules (Grotzinger et al. 2014; Stack et al. 2014). Drilling of the Sheepbed member provided images of gray mudstone tailings, in striking contrast with the dusty, red surface. Drill powders were delivered to CheMin and SAM, instruments onboard Curiosity that perform X-ray diffraction and evolved gas analyses, respectively (Blake et al. 2012; Mahaffy et al. 2012), with the aim of using mineralogical data and evolved volatile detections to constrain aqueous conditions during deposition (Vaniman et al. 2014; Ming et al. 2014). These data also bear on the nature and influence of post-depositional alteration with implications for the geological history of Gale and regional stratigraphic relationships of the sediments at YKB.

Methods: Mineralogical analysis

Curiosity is equipped with a suite of instruments used for direct and indirect mineralogical analysis (Blake et al. 2012; Campbell et al. 2012; Mahaffy et al. 2012; Wiens et al. 2012). Details of the instruments, data collection, and data reduction procedures are discussed in online supplemental materials[1], along with Appendix Figure 1[1].

[1] Deposit item AM-15-45077, Table 1, Appendix Figure 1, and Methods section. Deposit items are stored on the MSA web site and available via the *American Mineralogist* Table of Contents. Find the article in the table of contents at GSW (ammin.geoscienceworld.org) or MSA (www.minsocam.org), and then click on the deposit link.

Results

Bulk mineralogy

The bulk mineralogy of John Klein and Cumberland has been discussed by Vaniman et al. (2014) and is summarized here because it is relevant to discussions of the origins of clay minerals in the Sheepbed member. CheMin XRD patterns of both samples show similar crystalline, poorly crystalline phyllosilicate, and X-ray amorphous components (Fig. 1). The crystalline component largely consists of minerals expected from a basaltic source (plagioclase feldspar and pyroxenes). Accessory minerals include metal oxides and Ca-sulfates. Ca-sulfates may reside entirely in a series of fractures and veins observed in both drill holes. Fe-forsterite content in John Klein and Cumberland is 5.7 and 1.9 wt%, respectively, normalized to the crystalline component excluding clay minerals and the X-ray amorphous component. The analyzed Fe-forsterite content of John Klein may be abnormally high as a result of co-mingling of the John Klein sample with as much as 5% contamination by residue of a previous, olivine-rich sample, Rocknest, in the CHIMRA system. In any case, the quantity of Fe-forsterite in both samples is notably lower than estimates of olivine content of basalts in the Gale Region based on TES global mapping of 11 wt% (Rogers and Christensen 2007) and the 22 wt% olivine content of the nearby Rocknest aeolian sand shadow scooped and analyzed by Curiosity (Blake et al. 2013; Bish et al. 2013). Furthermore, the quantities of magnetite in the Sheepbed mudstone are high (8.7 and 9.5 wt% of the crystalline component at John Klein and Cumberland, respectively) given that sediments were deposited from non-turbulent suspensions in a lake as opposed to a vigorous fluvial setting that could have promoted physical density-driven sorting (Grotzinger et al. 2014; Vaniman et al. 2014; McLennan et al. 2014).

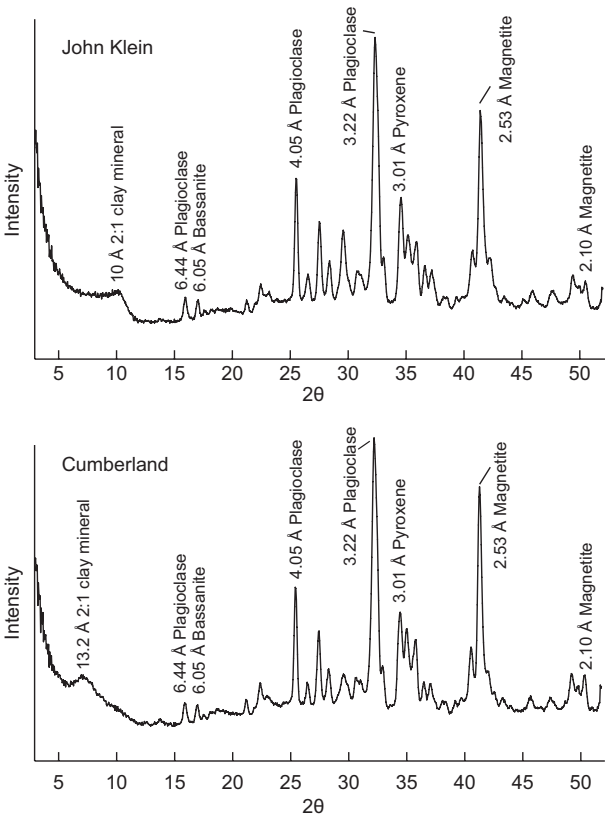

Figure 1. 1D XRD patterns from John Klein and Cumberland converted from 2D patterns, with the *d*-spacing and phase assignments labeled for major peaks. Diffractogram data were previously presented in Vaniman et al. (2014).

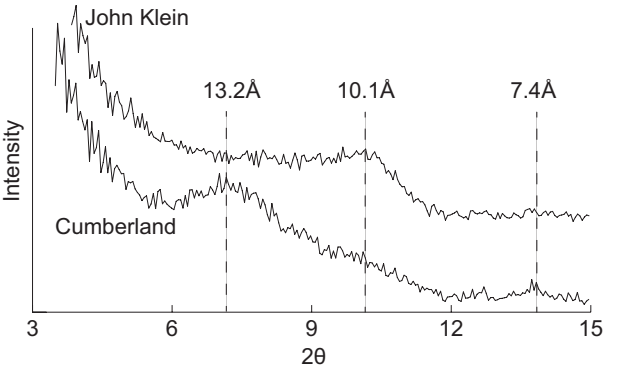

Figure 2. Comparison of John Klein and Cumberland XRD patterns in the clay mineral 001 region. Labeled basal spacings have been corrected to for Lorentz polarization.

Broad 00*l* diffraction peaks confirm the presence of clay minerals in John Klein and Cumberland. In the John Klein XRD pattern, a 001 reflection was observed between 8–11° 2θ Co*K*α (9.4 to 12 Å) with a Lorentz polarization corrected peak at ~10.1 Å, indicating the presence of 2:1 group clay minerals (Vaniman et al. 2014; Fig. 2). The 02*l* band of clay minerals lies between 22 and 23° 2θ and clearly contributes to the John Klein diffraction pattern, albeit with overlapping peaks from pigeonite and plagioclase (Vaniman et al. 2014; Fig. 3). A complex 001 peak in the Cumberland XRD pattern was observed between 6–11° 2θ (9.4 to 17 Å) with a Lorentz polarization corrected primary maxima at 13.2 Å (Vaniman et al. 2014). A weaker peak is centered at 10° 2θ Co*K*α (~10 Å) (Fig. 2). Like John Klein, Cumberland 00*l* peaks indicate the presence of 2:1 group clay minerals, albeit with a larger basal spacing (Vaniman et al. 2014). The 02*l* band of the Cumberland pattern appears to be in a similar position as John Klein (~22.5° 2θ, 4.58 Å) (Fig. 3).

The absence of 7 Å peaks in John Klein and Cumberland excludes the possibility of more than ~5 wt% contributions from chlorite, kaolin, and serpentine group minerals (detection limit estimated by Bish et al. 2013). A small peak at 7.4 Å observed in Cumberland is attributed to akaganeite (Vaniman et al. 2014). Talc and a disordered talc-like phase (kerolite) are members of the 2:1 clay mineral group, but they are unlikely to be present in YKB samples because the 00*l* peaks do not correspond, respectively, to the 9.38 and 9.65 Å spacing characteristic of these phases. Furthermore, the breadth of the ~10 Å 001 peak in John Klein is inconsistent with the presence of well-ordered mica.

The clay mineral content of John Klein and Cumberland is estimated at 22 and 18 wt%, respectively (±50% relative), based on whole-pattern fitting of the sample (Vaniman et al. 2014). Independent estimation of clay mineral content based on SAM EGA measurements of H_2O evolved during heating to

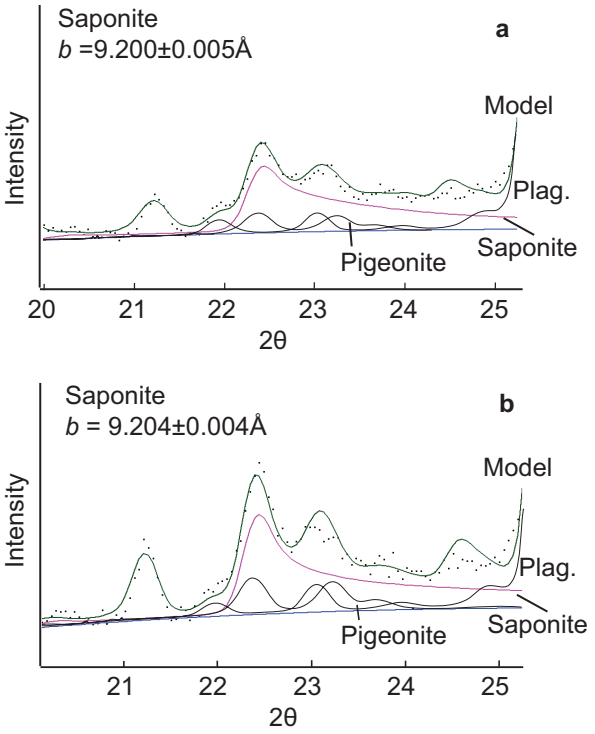

FIGURE 3. 02*l* region of John Klein (**a**) and Cumberland (**b**) XRD patterns showing data collected (black dots), and the modeled pattern (solid black line) calculated using Rietveld refinement showing contributions from saponite, pigeonite, and plagioclase (see description in text). Refined *b* unit-cell parameter of saponite is also shown.

temperatures that induce dehydroxylation indicate clay mineral contents of ~16–17 ± 11–12 wt% (McAdam et al. 2014, and in preparation).

Correct interpretation of basal reflections of clay minerals requires consideration of the differences in relative humidity (RH) on the floor of Gale crater and inside CheMin. Outside the rover RH ranges from close to 0% at midday to more than 70% at late night/early morning driven by temperature changes of up to 60 °C (Fig. 4). Theoretical work on the hydration states of montmorillonites predicts diurnal changes in interlayer hydration state under such conditions (Bish et al. 2003). In contrast, RH remains <1% inside CheMin because of warmer temperatures are maintained (ranging from 5–25 °C). Laboratory tests of the time taken for various expandable clay minerals to equilibrate in CheMin following changes in RH confirm they take place in a matter of hours to days (Rampe et al. in preparation). This is longer than similar changes in *d*-spacings of expandable clay minerals that occur within minutes when fully exposed to dry gas in conventional XRD instruments (e.g., Wilson et al. 2004). CheMin analyzed John Klein and Cumberland at intervals of 13 and 3 sols after drilling, respectively, so these samples should have attained equilibrium with the gas inside the instrument. To confirm this and to look for any other mineralogical changes that may have occurred inside CheMin, John Klein and Cumberland were re-analyzed at various times after initial analysis (see Table 1[1]). No changes were observed in positions of the basal reflections or other peaks of clay minerals.

John Klein

With these results in mind and considering that expandable clay minerals can collapse to ~10 Å under the low humidity conditions inside CheMin (Suquet and Pezerat 1987; Sato et al. 1992; Bish et al. 2003; Rampe et al. in preparation), the 00*l* peak observed at John Klein is permissive of the presence of discrete illite, discrete smectite, discrete vermiculite, mixed-layer illite-smectite (I/S), or mixed-layer talc-smectite (T/S).

Chemical constraints preclude illite as the major component species in John Klein. Mass-balance calculations using bulk-rock chemical data from APXS and the chemistry of crystalline components derived from unit-cell parameters (Vaniman et al. 2014; Morrison, in preparation) indicate a combined K_2O content of the clay mineral and amorphous components in John Klein of 0.69 wt%. K_2O content can be used to provide an upper bound on the discrete illite content of John Klein by assuming the all the clay mineral and amorphous component K is in discrete illite. Using a typical structural formula for illite, with 1.5 atoms of K per formula unit, discrete illite could potentially make up to ~25 wt% of the clay mineral fraction. However, given that much of the

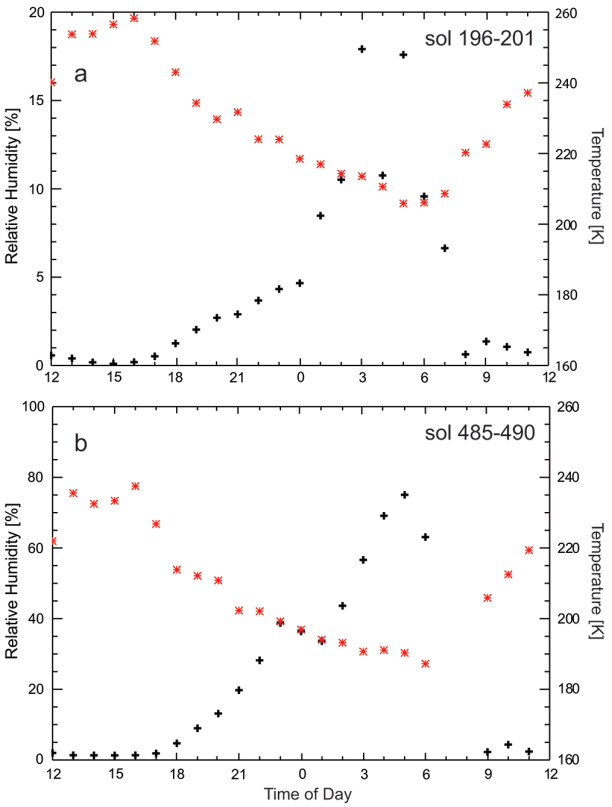

FIGURE 4. Relative humidity (black) and temperature data (red) from outside the rover (Planetary Data System Data Set ID for the REMS Instrument: MSL-M-REMS-5-MODRDR-V1.0). Data are averaged over 5 sol periods from sol 196–201 (**a**) and sol 485–490 (**b**) showing seasonal variability. RH inside CheMin, where temperatures are maintained between 5 to 20 °C remain <1%.

K could be partitioned into the amorphous material and K may also reside in exchangeable smectite interlayer sites, this upper estimate of illite content of John Klein is conservatively high.

The partially ordered stacking of illite gives rise to additional *hkl* peaks not seen in collapsed turbostratic smectite >23° 2θ (Co). It is not possible to evaluate the presence of these directly in the John Klein (and Cumberland) patterns because of the complexity induced by multiple crystalline phases and the amorphous component(s) that diffract/scatter in this region. However, whole-pattern fitting models of the John Klein XRD pattern including illite standards (Chipera and Bish 2002) did not improve fits, permissive evidence for the absence of discrete illite.

The 02*l* band maximum lies at ~22.5° 2θ (4.58 Å). This is most consistent with a trioctahedral clay mineral (Moore and Reynolds 1997), although it is noted that some synthetic Fe dioctahedral smectites have 02*l* bands positions close to the observed position in John Klein (Brigatti 1983; Heuser et al. 2013; Vaniman et al. 2014). Trioctahedral illites are uncommon on Earth (Galan 2006), and the few examples documented are transient weathering products of biotite in soils, often associated with vermiculite (Fordham 1990). Biotite was not detected in the Sheepbed mudstone and we consider the possibility of a source of biotite in the catchment remote given the basaltic nature of the crystalline mineral component observed in John Klein and Cumberland. Intermediate Mg-rich di-trioctahedral illites have been reported from ancient terrestrial saline lake deposits (Hover and Ashley 2003; Deocampo et al. 2009), but based on deconvolution of the 060 region of XRD patterns of terrestrial materials their 02*l* band positions would not match the Sheepbed clay minerals analyzed by CheMin.

Vermiculite typically forms from chlorite via chemical leaching. Chlorite was not detected by CheMin, and the bulk chemistry of the Sheepbed mudstone indicates little chemical alteration of sediments (McLennan et al. 2014), thus arguing against the presence of vermiculite in John Klein or Cumberland.

Mixed-layer I/S is typically dioctahedral, whereas mixed-layer trioctahedral smectites are usually intergraded with chlorite (Weaver 1989; Moore and Reynolds 1997). Thus, only small amounts of I/S are permitted by the chemistry and XRD pattern data, considered collectively. Another candidate mixed-layer clay mineral is talc/nontronite, reported from hydrothermally altered basalts in terrestrial seafloor settings (Cuadros et al. 2013). However, the mixed dioctahedral/trioctahedral nature of this phase gives rise to 02*l* bands with two peaks and two discreet dehydroxylation temperatures (Cuadros et al. 2013) not supported by current interpretations of XRD and SAM EGA data (Ming et al. 2014; McAdam et al. 2014, and in preparation).

Our favored interpretation is that the majority of the clay minerals in the John Klein sample are collapsed trioctahedral smectite with basal spacing of ~10 Å. Possible candidates include saponite (with some tetrahedral Al substitution for Si) and stevensite (which lacks tetrahedral Al substitution for Si). Unfortunately, precise information on the chemistry of the clay mineral is not available to make this distinction. However, a comparison of 02*l* band positions of clay mineral standards run on the CheMin 4 instrument, a reasonable proxy for the flight instrument that is similar in terms of operation and geometry (Sarrazin et al. 2005), indicates that ferrian saponite, informally known as Griffith Smectite (Treiman et al. 2015), is the closest of available materials in terms of 02*l* peak position. The peak release of water at ~750 °C is consistent with dehydroxylation of octahedral sheets of ferrian saponite (Fig. 5; Ming et al. 2014; McAdam et al. 2014, and in preparation). Additionally, ferrian saponite fits well with our proposed formation model (see below); reactive Al from the amorphous component of the Sheepbed mudstone was likely present during genesis, thus saponite is predicted (e.g., Bristow and Milliken 2011).

Cumberland

The low-angle region of the Cumberland XRD pattern is different from John Klein, in that it consists of a broad, complex peak between 9.4 to 17 Å with the highest intensity centered at 13.2 Å and a smaller rise around 10 Å. The 02*l* band position is virtually identical to that in John Klein. However, because determining the position of the 02*l* band can be complicated by interference of pigeonite and plagioclase *hkl* peaks (Fig. 2), its position was modeled using BGMN, a Rietveld refinement program that can generate XRD patterns of partially disordered clay minerals and consider contributions from other phases (Bergmann et al. 1998; Ufer et al. 2004). The position of the 02*l* band is related to the *b* unit-cell parameter of the clay mineral and Rietveld analysis shows the *b* parameter of clays from John Klein and Cumberland to be the same within error.

John Klein	$b = 9.200 \pm 0.005$ Å
Cumberland	$b = 9.204 \pm 0.004$ Å

The chemistry of individual crystalline mineral phases of John Klein, Cumberland, and the Rocknest sand shadow has

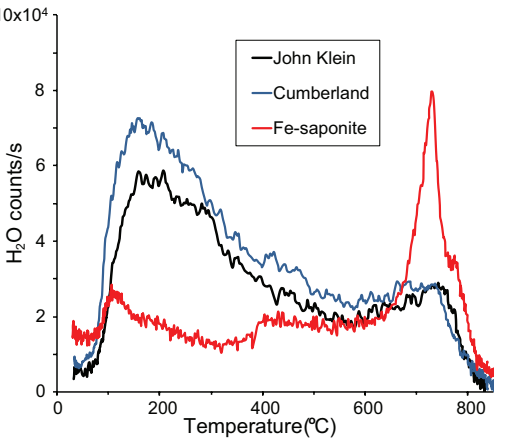

FIGURE 5. Evolved gas analysis of H_2O from a continuous ramp SAM pyrolysis of drill material from John Klein and Cumberland, compared with data from a ferrian saponite. The ferrian saponite tested is sample AMNH 89172 reported in Treiman et al. (2015). EGA data from the ferrian saponite were acquired under SAM-like conditions in the high-fidelity SAM Testbed laboratory instrument suite (McAdam et al. 2014, and in preparation). Because data from the main mass-to-charge ratio of H_2O (m/z 18, $H_2{}^{16}O$) were saturated, counts from H_2O isotopologs and fragments were plotted to illustrate H_2O signal vs. temperature [m/z 20 ($H_2{}^{18}O$) for John Klein and Cumberland and m/z 17 ×0.1 (OH fragment) for Fe-saponite].

been constrained based on unit-cell parameters determined by Rietveld refinement (Bish et al. 2013; Vaniman et al. 2014; Morrison et al. in preparation). This analysis is made possible by large databases that allow empirical relationships of mineral composition and unit-cell parameters to be derived (Morrison et al. in preparation). Similar attempts have been made to determine the influence of clay chemistry on the *b* unit-cell parameter of trioctahedral smectites based on statistical analysis (Brown and Brindley 1980). They are related as follows:

$$b\,(\text{trioctahedral}) = 9.18 + 0.06\text{Al}^{\text{IV}} - 0.12\,\text{Al}^{\text{VI}} - 0.06\text{Fe}^{3+} + 0.06\text{Fe}^{2+}$$

where Al^{IV}, Al^{VI}, Fe^{3+}, and Fe^{2+} are the proportions of Al and Fe atoms per $O_{10}(OH)_2$ in structural formulas, in tetrahedral, octahedral, ferric, and ferrous oxidation states, respectively. At the present time, calculated *b*-parameters for John Klein and Cumberland cannot be used to constrain detailed clay crystal chemistry without making major assumptions about the origin and magnitude of layer charge. However, available XRD data indicate that the clay minerals in John Klein and Cumberland are crystallographically similar, albeit exhibiting different swelling behavior. This similarity is expected given the fact that Cumberland and John Klein come from the same geological unit with similar mineralogy and are only 2.5 m apart with ~30 cm of stratigraphic separation.

Discussion

Swelling behavior

Possible explanations for the difference in 001 position and swelling behavior between the two Sheepbed samples include differences in the dominant interlayer cation present in the two samples and partial intercalation by metal-hydroxyl groups (i.e., incipient chloritization) in the Cumberland clay mineral (Vaniman et al. 2014), making it resistant to collapse within the <1% RH conditions of CheMin sample cells.

Smectites show variable hydration/dehydration properties depending on the type of interlayer cation as a result of differences in cation hydration energy. The two Sheepbed drill targets were deliberately chosen because they exhibit different diagenetic fabrics. John Klein is intensely fractured and filled with Ca-sulfate-bearing veins, whereas Cumberland is enriched in early diagenetic veins and nodules (Grotzinger et al. 2014). Thus, the clay minerals in these two samples may have been exposed to different fluids (or at least to different degrees) and may have different interlayer cations.

Of the possible cations found in expandable clays, the divalent cation Mg^{2+} is most effective at retaining interlayer H_2O. It is possible that the dominant interlayer cation in Cumberland is Mg because early diagenetic raised ridges nearby contain Mg-silicates that appear to have precipitated from fluids (Grotzinger et al. 2014; McLennan et al. 2014; Léveillé et al. 2014). However, experiments predict a single H_2O layer and basal spacing of about ~12.0 Å in Mg-bearing saponite (Suquet et al. 1975; Suquet and Pezerat 1987; Rampe et al. in preparation), inconsistent with observations from Cumberland. Vermiculite retains interlayer H_2O more effectively at low RH compared to saponite (Rampe et al. in preparation), but, as previously discussed, there is no XRD evidence for a vermiculite precursor in the Sheepbed member.

Based on the Ca-sulfate bearing vein content of John Klein, Ca^{2+} is a plausible prediction as the dominant interlayer cation, but Ca-bearing saponites also retain a single H_2O layer (~12.0 Å spacing) at low RH values (Suquet and Pezerat 1987; Ferrage et al. 2005; Rampe et al. in preparation). Based on the 10 Å 001 peak position and the discussions presented above that preclude illite, monovalent interlayer cations (Na^+ and/or K^+) may be prevalent in John Klein.

Our favored explanation for the lack of collapse in Cumberland is partial intercalation by metal-hydroxyl groups. On Earth, partial intercalation or chloritization of expandable clays is most commonly reported in acidic soils where conditions allow mobilization of hydroxy-Al that may be taken up in the interlayer (Rich 1968). Intercalation of hydroxy-Mg groups occurs in saline lake sediments exposed to alkaline Mg-rich waters (Jones and Weir 1983) and via neutral to mildly alkaline hydrothermal alteration (Pevear et al. 1982). Intercalation by Fe-hydroxyl groups is rarely observed but has been reported in reducing sediments that were subsequently exposed and oxidized (Lynn and Whittig 1966). Partially intercalated smectites, also known as intergrade smectite/chlorite, have a basal peak at ~13.5 Å and typically lack a measurable 002 peak at ~7 Å. It is possible that the weak 10 Å peak in the Cumberland pattern represents a fraction that has not been intercalated by metal-hydroxyl groups.

Origin of clay minerals

Fe/Mg-smectites are the most common types of clay minerals observed on Mars by global spectroscopic surveys (Ehlmann et al. 2011). The dominantly mafic composition of the martian crust and multiple mechanisms and instances in which moderate pH fluids can interact with abundant, reactive Fe and Mg silicate minerals ensures this (Bristow and Milliken 2011). Thus, determining whether the clay minerals in the Sheepbed mudstone are detrital or formed in place is challenging (Milliken and Bish 2010; Bristow and Milliken 2011).

Chemical and mineralogical data collected by MSL provide evidence of an in situ origin for Sheepbed clay minerals. The bulk rock chemistry of the Sheepbed member is not significantly different from average martian basalt (McLennan et al. 2014). Transport and hydrodynamic sorting of clay mineral-bearing sedimentary detritus during deposition of the Sheepbed member would likely have fractionated minerals and produced changes in chemistry relative to other Sheepbed units, but this is not observed (McLennan et al. 2014). Instead, low water:rock alteration in a system with little chemical transport is indicated. Consistent with this scenario, the low forsterite content of John Klein and Cumberland (estimated at 5.7 and 1.9 wt% of the basaltic detritus) suggests that the clay minerals in the Sheepbed mudstone are largely derived from aqueous alteration of olivine, involving minimal loss of chemical components (McLennan et al. 2014; Vaniman et al. 2014). Given their sedimentary context, the high levels of magnetite (8.7 and 9.5 wt% of crystalline phases other than smectite for John Klein and Cumberland, respectively) are hypothesized as a second product of the olivine alteration reaction (McLennan et al. 2014; Vaniman et al. 2014).

In the absence of active removal of chemical components, hydration of olivine to produce clay minerals plus magnetite

involves a significant increase in volume. Signs of brittle deformation expected in a lithified host were not observed in the Sheepbed mudstone. Instead, the early diagenetic raised-ridges observed in the Sheepbed member (Grotzinger et al. 2014) are thought to be a response to volume changes induced by production of clay minerals prior to lithification of the Sheepbed mudstone (Siebach et al. 2014).

An alternative hypothesis for the clay minerals at YKB is that they are predominantly detrital materials sourced from the northern walls and rim of Gale crater. Indeed, clay minerals have been detected in the walls of Gale crater (Wray 2013) and in the bedrock of the region (Ehlmann and Buz 2015). Possible modes of detrital clay mineral formation include; (1) weathering, (2) hydrothermal activity related to the impact that created Gale (Schwenzer et al. 2012), and (3) regional subsurface aqueous activity prior to formation of Gale (following Ehlmann et al. 2011).

In our opinion, inputs of detrital clay minerals at YKB produced via impact-related hydrothermal alteration (Schwenzer et al. 2012) and/or weathering in the source region were minimal. This inference is based on comparing the quantity and types of clay minerals in the YKB assemblage with observations and predictions from impact-related hydrothermal systems and weathering profiles.

An impact big enough to form a crater the size of Gale would have induced high-temperature gradients and, given sufficient water supply, sustained hydrothermal alteration in the crater rim lasting up to hundreds of thousands of years (Abramov and Kring 2005). Based on terrestrial data from impacts and geochemical modeling, a heterogeneous assemblage of clay alteration products, potentially including nontronite, celadonite, corrensite, chlorite, mica, talc, and mixed-layer minerals composed of these end-members could result from such processes with steep temperature and fluid gradients (Hagerty and Newsom 2003: Schwenzer et al. 2012). The simple clay mineral assemblage of the Sheepbed member is not easily reconciled with such a source.

Saponite is generally produced during the early stages of hydrolytic weathering of basalt when Fe, Mg, and Si activities are high (Meunier 2005; but see Ziegler et al. 2003 for an exception where halloysite is the main product from inception of arid-zone basalt weathering). However, saponite does not typically form in isolation; and the mosaic of microenvironments within weathering profiles can generate other dioctahedral 2:1 phyllosilicates such as celadonite, Fe-beidellite and nontronite during early basalt weathering (Meunier 2005; Garcia-Romero et al. 2005), minerals not detected by CheMin at YKB. Moreover, the abundance of secondary phases found at YKB, with clay minerals making up ~20 wt% of the mudstone (Vaniman et al. 2014), suggest an extensive degree of alteration in any hypothetical weathering profile. Mature basaltic weathering profiles often give kaolinitic clay minerals and goethite (Meunier 2005), also not observed at YKB.

The clay mineral products of widespread Noachian subsurface alteration of thick sections of martian crust hypothesized by Ehlmann et al. (2011) cannot be entirely ruled out as potential detrital source of clay minerals at YKB. However, CheMin has not detected predicted accompanying phases such as zeolites (Ehlmann et al. 2011), which would strengthen the case for such a source.

In some low-temperature terrestrial sedimentary basins, strongly saline, acidic or alkaline fluids are capable of overprinting/transforming detrital clay minerals, thus, altering clay mineral assemblages to reflect ambient conditions prior to lithification (Jones and Spencer 1999; Larsen 2008; Bristow et al. 2012). The Sheepbed mudstone lacks significant quantities of chemical phases (with the exception of later vein fills) that would be expected in saline or acidic lacustrine systems (Bristow and Milliken 2011; Bowen et al. 2012; McLennan et al. 2014). Alkaline conditions (pH 9–10) could potentially explain the partial intercalation of Cumberland smectites by metal-hydroxide groups in addition to homogenizing clay mineral assemblage, but the Sheepbed mudstone lacks other authigenic mineral indicators, like zeolites, K-feldspars, and carbonates that are characteristic of alkaline systems (Bristow and Milliken 2011).

Timing of clay mineral formation

The kinetics of olivine dissolution at low temperatures is consistent with the alteration of olivine to a clay mineral prior to lithification of the Sheepbed mudstone. Olivine dissolution, the first step in the formation of secondary phases, is influenced by various factors including grain size, pH, olivine composition, chemistry of fluids and atmosphere, as well as temperature (Stopar et al. 2006; Olsen and Rimstidt 2007; Hausrath and Brantley 2010). Broad constraints are available for many of these governing factors, including: (1) grain size <50 μm (Grotzinger et al. 2014), (2) remnant olivine composition (estimated as Fo_{46} in the Sheepbed mudstone; Vaniman et al. 2014), and (3) the persistence of clay minerals (excludes pH extremes and brackets fluid pH in the ~5–9.5 range). The lifetime of olivine in such a system could range from thousands to hundreds of thousands of years at temperatures between 0 and 25 °C, when considering field dissolution rates are typically 100× slower than laboratory rates (Stopar et al. 2006; Olsen and Rimstidt 2007). These durations overlap with the estimated depositional period of hundreds to tens of thousands of years for the Sheepbed member (Grotzinger et al. 2014). Indeed, it is plausible that the YKB formation is part of a much thicker stack of fluvio-lacustrine strata representing water activity over a period of millions to tens of millions of years (Grotzinger et al. 2014), providing ample time in situ for clay mineral production. We also note that other abundant basaltic minerals in the Sheepbed mudstone (pyroxenes and plagioclase) have lifetimes that are orders of magnitude greater than olivine under surficial conditions (Hausrath et al. 2008), consistent with their persistence in the Sheepbed member.

Clay mineral diagenesis?

XRD data suggest that YKB smectites have not undergone detectable diagenetic changes typically associated with thermal alteration that often promotes the transformation of saponite into corrensite, an ordered mixed-layer trioctahedral smectite/chlorite (Chang et al. 1986; Meunier 2005; Derkowski et al. 2013). The ordered interstratification of smectite and chlorite yields a 001 supercell peak corresponding to a spacing of 14.2 Å (chlorite layer) plus the spacing of the smectite layers (Moore and Reynolds 1997). Thus peaks at ~24 and ~28 Å would be present for John Klein and Cumberland, respectively, if ordered corrensite was present; these supercell peaks were not observed. However,

chlorite/smectite interstratifications may be poorly ordered, and supercell peaks are therefore not always expected products of prograde diagenesis of saponite. In summary, minor amounts (estimated at <5 wt% of the bulk sample because of increased low angle scattering) of corrensite in the Sheepbed samples could remain undetected by CheMin.

The partial intercalation of metal-hydroxyl groups suggested by the expanded basal reflection in Cumberland is distinct from the true mixed-layer chlorite/smectites expected from prolonged thermally induced diagenesis. The Sheepbed member has experienced an episode of fluid induced fracturing post-lithification, with fractures then filled by Ca-sulfates. This does not appear to have caused the partial metal-hydroxyl intercalation of the clay minerals in Cumberland. As discussed previously, rock permeability and porosity are likely to have been occluded during early diagenesis (McLennan et al. 2014). Moreover, the fluids were enriched in Ca, rather than Mg, Al, or Fe, which are necessary to form intercalated metal-hydoxyl groups in the clay minerals. In addition, fracture density is higher in John Klein than Cumberland, while intercalation is only apparent in Cumberland

Parts of the Sheepbed member contain early diagenetic raised ridges (Siebach et al. 2014), which bear Mg-silicate cements tentatively assigned as Al-poor Mg-phyllosilicates based on chemical compositional analysis by APXS and ChemCam (McLennan et al. 2014; Léveillé et al. 2014). We propose that the fluids from which these cements precipitated induced partial intercalation of saponites at Cumberland. Direct precipitation of Mg-clay minerals at low temperatures requires either high-pH or high-Mg activities in solution (Bristow and Milliken 2011) plus a source of aqueous SiO_2; these conditions are expected to promote partial intercalation of pre-existing smectites.

Origin of magnetite

Like saponite, magnetite is proposed to be authigenic in origin (Vaniman et al. 2014; McLennan et al. 2014). Enrichment via hydrodynamic sorting is excluded because overlying sandstones, where hydrodynamic concentration of heavy minerals is expected to be most pronounced, do not contain significant magnetite, as indicated by their Fe content (McLennan et al. 2014). In addition, other elemental indicators provided by APXS analysis of the Sheepbed mudstone do not support enrichment of heavy minerals by sedimentary processes (McLennan et al. 2014). Production of magnetite has been tentatively tied to saponite production during the alteration of olivine (Vaniman et al. 2014) in a process that may be analogous to aqueous alteration of olivine and mesostasis or impact glass observed in certain chondrites and martian meteorites (Tomeoka and Buseck 1990; Treiman et al. 1993; Keller et al. 1994).

The reaction also invites comparisons with reactions involved in the serpentinization of ultramafic rocks on Earth, in which olivine is hydrated, forming serpentine-group phyllosilicates, magnetite, and hydrogen (under some conditions; see McCollom and Bach 2009; Klein et al. 2013). Saponitic clay minerals are not observed in typical serpentinization assemblages (Evans et al. 2013) because their formation requires the addition of Si and Al. In meteorites, these constituents are supplied via reaction with mesostasis or impact glass, and it is possible that the Si- and Al-bearing X-ray amorphous material, ~30 wt% of the Sheepbed mudstone, was a source (Morris et al. 2013).

Given the isochemical nature of the proposed clay mineral formation reaction, mass balance between reactants and products is expected. Thus, estimated quantities of saponite determined from CheMin data can be used to back-calculate olivine consumed and expected quantities of magnetite co-produced. Two scenarios are presented in Table 2. In both, it is assumed that 18 wt% saponite (the quantity observed in Cumberland) forms with magnetite by aqueous reaction of Fo_{50} olivine and SiO_2 and Al_2O_3 from the amorphous component. In the first scenario, the saponite has a structural formula that closely approximates the Clay Minerals Society's source clay saponite standard SapCa-2 [$Mg_3(Si_{3.6}Al_{0.4})O_{10}(OH)_2$]. In the second, the structural formula is a ferrian saponite with a composition approximating material from Griffith Park, California [$Mg_2Fe^{3+}(Si_{3.4}Al_{0.6})O_{10}(OH)_2$; Treiman et al. 2015]. The quantities of magnetite calculated to form with ferrian saponite are close to observed amounts, 3.4 vs. 4.4 wt% of the whole Cumberland sample, respectively. The small difference could be accounted for by small quantities of detrital magnetite in the Sheepbed mudstone and/or errors in mineral quantification based on profile modeling of the XRD data. The in situ formation of ferrian saponite requires consumption of ~15 wt% olivine, which is reasonable given orbital estimates of basalt olivine content in the YKB/Gale crater region and olivine content present in martian basalts and soils (Rogers and Bandfield 2009; Bish et al. 2013; Blake et al. 2013). The production of a Fe-free saponite like SapCa-2 at YKB (reaction 1, Table 2) is less likely given the large amounts of magnetite produced (11 wt%) by this reaction and the need for more olivine (~25 wt%).

If this "saponitization" reaction took place within the Sheepbed mudstone it raises the possibility of H_2 production within sediments. Generation of H_2 may help explain void-bearing early diagenetic concretions ("hollow nodules") observed in the Sheepbed member (Grotzinger et al. 2014). More importantly, H_2 would have been a potential energy source for chemolithoautotrophic organisms (Grotzinger et al. 2014; Vaniman et al. 2014).

However, studies of serpentinizing systems give rise to questions about the thermodynamic viability of producing significant H_2 from alteration of olivine to magnetite at temperatures less than ~100 °C. Although phyllosilicate production proceeds, thermodynamic reaction models of olivine serpentinization (at low SiO_2 activities) suggest that formation of magnetite below 100 °C is unfavorable. This limits the production of H_2 because less Fe is oxidized by water and what little Fe^{3+} is produced is partitioned into Fe^{3+} hydroxide (McCollom et al. 2009; Klein et al. 2013; Mayhew et al. 2013). Empirical studies of low-temperature serpentinization reactions confirm reaction models with Fe^{3+} hydroxide and ferrobrucite, the main Fe-bearing reaction products at 55 °C (Mayhew et al. 2013). These experiments also indicate that spinel-group minerals provide an important pathway for the oxidation of Fe by water with production of H_2 (Mayhew et al. 2013).

The thermodynamic modeling approach has been adapted to simulate hypothesized reactions at YKB. In these simulations, fayalite was reacted with SiO_2 and Al_2O_3, to mimic posited reactive components of the X-ray amorphous phase, with reducing solutions containing small amounts of sodium chloride using

Geochemist Work Bench (Table 3). In this batch of simulations anoxic conditions were prescribed because they predominate in serpentinization systems. The influence of variable oxygen availability is described later in this paper. End-member fayalite was used as a reactant even though the olivine at YKB is probably Fe-forsterite (Vaniman et al. 2014), because GWB is not optimized for dealing with solid solutions. Moreover, previous studies indicate that magnetite forms at lower temperatures from fayalite compared to more Mg-rich olivines (Klein et al. 2013). The standard thermodynamic database for GWB 9.0.7 was modified to contain ferrous saponite data from Wilson et al. (2006). The simulations suggest that the addition of reactive SiO_2 and Al_2O_3 does not influence the temperature at which magnetite becomes a significant part of the alteration assemblage and H_2 is produced in this type of reaction (Table 3).

Based on current knowledge, production of several weight percent magnetite at surficial temperatures shortly after sedimentation via "saponitization" is improbable. It is possible to envisage olivine initially reacting to form saponite and Fe-hydroxides or other poorly crystalline Fe-oxyhydroxide phases that later matured to magnetite under more favorable higher-temperature conditions. However, considering maximum potential burial depth and estimated geothermal gradients, in addition to the absence of prograde diagenetic clay minerals corrensite and chlorite, the Sheepbed member was probably not heated above 75 °C (Vaniman et al. 2014).

Evidence of a possible low-temperature pathway comes from studies of aqueous olivine alteration to assemblages of saponite and magnetite in martian meteorites (e.g., Treiman et al. 1993), although we note this style of alteration is not entirely analogous to YKB because it only affects up to about 1% of some SNC meteorites. For instance, in the nakhlites, there is a succession of siderite–saponite–minor Fe oxide–saponitic gel interpreted as post-impact hydrothermal alteration starting with a high-temperature carbonate forming phase and cooling to about 50 °C before forming saponite and serpentine (Changela and Bridges 2010; Bridges and Schwenzer 2012). The Fe-rich saponite and saponitic composition gel identified in the nakhlites has been shown through X-ray absorption spectroscopy to be ferric (Hicks et al. 2014), indicating oxidizing conditions. Further exploration of the influence of different host rocks and mineral mixtures on clay mineral formation at YKB (based on nakhlite martian meteorites) is presented within an accompanying paper (Bridges et al. 2015).

In the Bali CV3 chondrite, saponite and magnetite preferentially form in planar defects of olivine crystals that were subject to oxidation and partial conversion to Fe^{3+}-oxides during magmatic cooling (Keller et al. 1994). Laboratory genesis of magnetite at room temperature and near neutral pH requires aqueous Fe^{2+} and small amounts of oxidants, either Fe^{3+} from dissolution of ferrihydrite or air bubbled through solutions (Taylor et al. 1987). Such conditions have been likened to those found in soils that bear enrichments of authigenic magnetite (e.g., Maher and Taylor 1988).

A slight modification of our reaction path models that includes modest additions of $O_{2(aq)}$ confirms these empirical and petrological observations (Table 4). In these models magnetite and saponite are produced at 5 °C through moderate oxidation of Fe^{2+} (Table 3). Only a trace of $H_{2(aq)}$ is produced and is independent of the amounts of magnetite produced. At higher [$O_{2(aq)}$] [20 mmol/kg $O_{2(aq)}$ using the conditions prescribed in Table 3] hematite and gibbsite are produced at the expense of magnetite and clay minerals and the pH at the end of the reaction drops compared to reactions with lower [$O_{2(aq)}$] (Table 4).

Table 2. Mass-balance calculation for reaction between olivine and water to form saponite and magnetite

	Saponite observed	Magnetite produced	Fo_{50} olivine required
Reaction 1	18 wt%	11%	24.5%
Reaction 2	18 wt%	3.4%	15.1%

Note: Both reactions require balancing via addition of oxidants as reactants or production of hydrogen gas—discussed in the text. Reactions:
(1) $2.8H_2O + 0.6SiO_2(aq) + 0.4Al^{3+}(aq) + 3MgFeSiO_4 \rightarrow Fe_3O_4 + Mg_3(Si_{3.6}Al_{0.4})O_{10}(OH)_2$ [saponite].
(2) $2.53H_2O + 1.4SiO_2(aq) + 0.6Al^{3+}(aq) + 2MgFeSiO_4 \rightarrow 0.33Fe_3O_4 + Mg_2Fe^{3+}(Si_{3.4}Al_{0.6})O_{10}(OH)_2$ [Fe^{3+} saponite].

Table 3. Results of thermodynamic reaction modeling of "saponitization" under anoxic conditions at various water:rock ratios (W:R)

Temperature	10 °C	50 °C	90 °C	130 °C
	W:R = 1			
Fe-saponite (wt%)	73.4	73.5	74.0	87.8
Chlorite (wt%)	5.7	5.7	5.6	2.2
Serpentine (wt%)	20.9	20.8	20.3	4.8
Magnetite (wt%)	trace	trace	0.2	5.2
H_2(aq) (mmol/kg)	0.06	0.5	9.5	245
	W:R = 10			
Fe-saponite (wt%)	73.5	73.8	79.2	92.1
Chlorite (wt%)	5.7	5.6	4.3	1.2
Serpentine (wt%)	20.8	20.5	14.4	
Magnetite (wt%)	trace	trace	2.1	6.7
H_2(aq) (mmol/kg)	0.06	0.5	9.5	30.4
	W:R = 100			
Fe-saponite (wt%)	74.2	77	92.1	92.1
Chlorite (wt%)	5.5	4.8	1.1	1.1
Serpentine (wt%)	20.1	17		
Magnetite (wt%)	0.2	1.2	6.8	6.8
H_2(aq) (mmol/kg)	0.06	0.06	3	3

Notes: The production of magnetite and H_2 only occurs to a significant extent above ~75 °C. A similar temperature dependence is familiar from previous work on serpentinizing systems (McCollom et al. 2009; Klein et al. 2013). Starting solution composition: Fe^{2+} = 0.1 mmol/kg, $SiO_{2(aq)}$ = 0.1, Cl^- = 1.2 mmol/kg (free to balance charge), Al^{3+} = 0.001 mmol/kg, Na^+ = 1 mmol/kg, $O_{2(aq)}$ = 0.01 mmol/kg, pH = 7.

Table 4. Thermodynamic reaction modeling of aqueous alteration of fayalite, Al_2O_3, and SiO_2, with variable amounts of $O_{2(aq)}$

$O_{2(aq)}$ reacted (mmol/kg)	0	1	5	10	15	20
	W:R = 10, *T* = 5 °C					
Fe-saponite (wt%)	73.5	74.6	79.6	86.2	91.9	92.7
Chlorite (wt%)	5.7	5.4	4.2	2.7	1.2	
Serpentine (wt%)	20.8	19.5	14.0	7.1	0.1	
Magnetite (wt%)	trace	0.5	2.2	4.4	6.7	3.3
Gibbsite (wt%)						0.2
Hematite (wt%)						3.8
pH	8.2	8.6	8.6	8.6	8.6	7.8
$H_{2(aq)}$ (mmol/kg)	0.05	0.05	0.05	0.05	0.05	trace

Note: Starting solution composition: Fe^{2+} = 0.1 mmol/kg, $SiO_{2(aq)}$ = 0.1, Cl^- = 1.2 mmol/kg (free to balance charge), Al^{3+} = 0.001 mmol/kg, Na^+ = 1 mmol/kg, $O_{2(aq)}$ = 0.01 mmol/kg, pH = 7.

Terrestrial analogs

To the best of our knowledge, an exact low-temperature terrestrial analog for the Sheepbed mudstone has not been documented. However, assemblages of authigenic magnetite and smectite have been reported from Eocene age iron-meromictic

lake sediments in the Seward Peninsula, Alaska (Dickinson 1988). The basaltic flows that dammed regional drainage, resulting in lake formation, also served as a source of Fe in lake waters and pore-fluid (Dickinson 1988). Hollow magnetite spherules up to 0.9 mm in diameter with a proposed authigenic origin are reported from recent sediments (<20 000 yrs old) of volcanic crater lake Barombi Mbo in West Cameroon (Cornen et al. 1992). Here magnetite coexists with authigenic brown granules consisting of kaolinite and Fe-hydroxides. Lake sediments are supplied with basaltic detritus including olivine from the catchment via streams and ash falls (Cornen et al. 1992).

Low-temperature authigenic magnetite formation within the Sheepbed member would require moderate levels of oxidants to react with Fe^{2+} derived from the dissolution of fine-grained olivine detritus. Possible sources that could maintain such levels include the diffusion of O_2 from the atmosphere, a supply of Fe^{3+} from dissolution of detrital material, or photochemical production of Fe^{3+} within the water column (Hurowitz et al. 2010). It is possible that the waters of YKB contained sulfate that served as an oxidant. Oxidized and reduced forms of sulfur and perchlorates are detected by CheMin and SAM in the Sheepbed mudstone (Vaniman et al. 2014; Ming et al. 2014), but it is unclear as to what proportions of these species were part of the original depositional system as opposed to being introduced during later diagenesis that resulted in sulfate-filled veins. Whatever the chemical pathway, the presence of saponites indicates that the degree of Fe^{2+} oxidation was moderate, and thus avoided reducing the pH to the point where acidic conditions inhibited smectitic clay formation and preservation was no longer favorable. Fe^{2+} oxidation could potentially be limited by rapid partitioning into authigenic magnetite and clay minerals.

IMPLICATIONS

Geological context of the Yellowknife Bay Formation

Part of Curiosity's ongoing mission is to determine how the rock units the rover encounters fit into a wider geological context of Gale crater. This is of particular importance for the YKB formation because collective evidence indicates that the strata represent an ancient environment potentially capable of supporting life (Grotzinger et al. 2014). Thus, determining the relationship between the YKB formation, the Peace Vallis fan, and the strata at the base of Mt. Sharp have implications for its age and help define periods in martian history when the planet was habitable (Grotzinger et al. 2014).

On Earth, clay mineralogy is widely used as a tool for reconstructing the burial history of sedimentary basins. Thus, it is also worth considering whether YKB clay minerals could provide constraints that help place the YKB strata in a regional context. In terrestrial sedimentary basins, saponite is chloritized to corrensite during burial diagenesis at temperatures as low as 60–70 °C (Chang et al. 1986). However, the local chemical environment and duration of heating have a significant influence and conversion to corrensite may not occur until 160 °C in some basins (Meunier 2005). The early occlusion of permeability and porosity in the Sheepbed member may have also inhibited clay mineral diagenesis (e.g., Derkowski et al. 2013), in combination with dry conditions in Gale crater after clay mineral formation (Tosca and Knoll 2009).

In addition to the inherent complexities of trying to use the alteration of saponites as a paleothermometer, significant differences in geothermal gradients are expected between Earth and Mars, given the thicker martian lithosphere and absence of plate tectonics. A geothermal gradient of 15 °C/km is estimated for Gale crater during the Late Noachian/Early Hesperian (Hahn et al. 2011). The result is that a complex and prolonged history of burial, compaction, fluid circulation, and cementation is possible in the YKB formation with minimal heating. Indeed, comparisons of the YKB formation with first-cycle basaltic sediments on Earth may be particularly difficult given Earth's active tectonic settings and elevated geothermal gradients.

Strata at the base of Mt. Sharp may have been buried to depths of up to 5 km (Malin and Edgett 2000), corresponding to an estimated temperature of 75 °C (Hahn et al. 2011), and would likely have spent millions of years at this depth before being exposed by wind erosion (Malin and Edgett 2000). Indeed, Farley et al. (2014) calculated a surface exposure age of 78 ± 30 million years. Such conditions would not necessarily lead to the chloritization of saponite. Thus the absence of detectable corrensite in the Sheepbed mudstone does not preclude a relationship between the YKB formation and basal strata of Mt. Sharp.

It is also notable that orbitally detected clay minerals in strata at the base of Mt. Sharp are identified as nontronite (Milliken et al. 2010), a variety of Fe-rich dioctahedral smectite that appears to be distinct from clay minerals discovered in the Sheepbed mudstone. Differences in clay mineralogy do not exclude the possibility that the YKB formation is part of the same sedimentary system exposed at the base of Mt. Sharp. The clay minerals in these two areas could simply reflect differences in authigenic pathways influenced by local conditions or reflect variable proportions of authigenesis vs. detrital inputs (Bristow and Milliken 2011). Moreover, the clay minerals in Mt. Sharp may be secondary rather than depositional or authigenic materials. Future investigations by Curiosity at Mt. Sharp will help resolve these issues.

Mineralogic constraints on habitability

The clay minerals and authigenic magnetite discovered in the Sheepbed mudstone provide critical paleoenvironmental constraints. Their formation and persistence are evidence of aqueous alteration of basaltic detritus at moderate pH (Vaniman et al. 2014; Grotzinger et al. 2014). The additional discussion of olivine alteration kinetics presented here indicates the persistence of circum-neutral, moderately oxidizing aqueous conditions at YKB for thousands to hundreds of thousands of years. This provides a first-order minimum constraint on the time available for any life to establish itself in this ancient fluvio-lacustrine system.

The evidence presented here for low-temperature production of saponite and magnetite by controlled oxidation of Fe^{2+} from dissolved olivine also suggests potential available energy sources for life inhabiting the muddy lake sediments of YKB. On Earth, neutrophilic iron-oxidizing bacteria and archaea are found in a range of habitats. Chemolithotrophic microaerophiles grow at oxic/anoxic interfaces using soluble Fe^{2+} as their energy source (Edward et al. 2004; Emerson et al. 2010), while anaerobic organisms couple Fe^{2+} oxidation to nitrate reduction (Straub

and Buchholz-Cleven 1998) and photoautotrophy (Widdel et al. 1993; Croal et al. 2004). Microaerophilic microbial communities are known to couple Fe^{2+} oxidation to Fe^{3+} reduction (e.g., rhizosphere of wetland plants; Weiss et al. 2003). Such microscale iron cycles are supported by anaerobic Fe^{3+} reducers such as *Geobacter metallireducens* that can couple the reduction of insoluble Fe^{3+} to the oxidation of a wide range of organic molecules (Lovly, et al. 1993). Perhaps most relevant to YKB are isolates of Fe-oxidizer *Pseudomonas* sp. HerB from the rock-ice interface of a lava-tube cave in Oregon that use olivine as a source of energy under the low oxygen conditions envisioned within the Sheepbed mudstone (Popa et al. 2012).

H_2 may have been produced through low-temperature reactions of water and olivine or in anoxic microenvironments within the sediments at YKB (Stevens and McKinley 2000; Neubeck et al. 2011; Mayhew et al. 2013). H_2 is a viable electron donor in a range of metabolic pathways; however, laboratory and terrestrial field observations identify H_2 production rates close to the limits of survival of archaea where water and olivine react at low temperatures (Stevens and McKinley 2000; Neubeck et al. 2011). Thus, H_2 was, at best, a secondary potential biotic energy source.

Acknowledgments

We are grateful to R. Kleeburg for help with modeling XRD patterns and to D. Deocampo and J. Cuadros for thoughtful reviews. Support from the engineers and staff of NASA Mars Science Laboratory Mission are gratefully acknowledged. Part of this research was carried out at the Jet Propulsion Laboratory, California Institute of Technology, under a contract with the National Aeronautics and Space Administration.

References cited

Abramov, O., and Kring D.A. (2005) Impact-induced hydrothermal activity on early Mars. Journal of Geophysical Research, 110, E12S09, http://dx.doi.org/10.1029/2005JE002453.

Anderson, R.B., and Bell, J.F. III (2010) Geologic mapping and characterization of Gale crater and implications for its potential as a Mars Science Laboratory landing site. Mars, 5, 76–128.

Anderson, R.C., Jandura, L., Okon, A.B., Sunshine, D., Roumeliotis, C., Beegle, L.W., Hurowitz, J., Kennedy, B., Limonadi, D., McCloskey, S., Robinson, M., Seybold, C., and Brown, K. (2012) Collecting samples in Gale crater; an overview of the Mars Science Laboratory sample acquisition, sample handling and processing system. Space Science Reviews, 170, 57–75.

Bergmann, J., Friedel, P., and Kleeberg, R. (1998) BGMN a new fundamental parameter-based Rietveld program for laboratory X-ray sources, its use in quantitative analysis and structure investigations. Commission of Powder Diffraction, International Union of Crystallography. CPD Newsletter, 20, 5–8.

Bibring J-P., Langevin Y., Mustard, J.F., Poulet, F.O., Arvidson, R., Gendrin, A., Gondet B., Mangold, N., Pinet, P., Forget, F., and others. (2006) Global mineralogical and aqueous Mars history derived from OMEGA/Mars Express data. Science, 312, 400–404.

Bish, D.L., Carey, J.W., Vaniman, D.T., and Chipera, S.J. (2003) Stability of hydrous minerals on the martian surface. Icarus, 164, 96–103.

Bish, D.L., Blake, D.F., Vaniman, D.T., Chipera, S.J., Morris, R.V., Ming, D.W., Treiman, A.H., Sarrazin, P., Morrison, S.M., Downs, R.T., and others. (2013) X-ray results from Mars Science Laboratory: Mineralogy of Rocknest at Gale crater. Science, 341, 1238932, http://dx.doi.org/10.1126/science.1238932.

Blake, D.F., Vaniman, D.T., Achilles, C.N., Anderson, R., Bish, D., Bristow, T., Chen, C., Chipera, S., Crisp, J., Des Marais, D., and others. (2012) Characterization and calibration of the CheMin mineralogical instrument on Mars Science Laboratory. Space Science Reviews, 170, 341–399.

Blake, D.F., Morris, R.V., Kocurek, G., Morrison, S.M., Downs, R.T., Bish, D., Ming, D.W., Edgett, K.S., Rubin, D., Goetz, W., and others. (2013) Curiosity at Gale crater, Mars: Characterization and analysis of the Rocknest sand shadow. Science, 341, 1239505, http://dx.doi.org/10.1126/science.1239505.

Bowen, B.B., Benison, K.C., and Story, S. (2012) Early diagenesis by modern acid brines in Western Australia and implications for the history of sedimentary modification on Mars. In J.P. Grotzinger and R. Milliken, Eds., Mars Sedimentology, SEPM Special Publication, 102, 229–252.

Bridges, J.C., and Schwenzer, S.P. (2012) The nakhlite hydrothermal brine. Earth and Planetary Science Letters, 359, 117–123.

Bridges, J.C., Schwenzer, S.P., Leveille, R., Westall, F., Wiens, R.C., Mangold, N., Bristow, T., Edwards, P., and Berger, G. (2015) Diagenesis and clay mineral formation at Gale Crater, Mars. Journal of Geophysical Research: Planets, in press, http://dx.doi.org/10.1002/2014JE004757.

Brigatti, M.F. (1983) Relationships between composition and structure in Fe-rich smectites. Clay Minerals, 18, 177–186.

Brindley, G.W., and Lemaitre. J. (1987) Thermal oxidation and reduction reactions of clay minerals. In A.C.D. Newman, Ed., Chemistry of Clays and Clay Minerals, Mineralogical Society Monograph, 6, 319–370.

Bristow, T.F., and Milliken, R.E. (2011) Terrestrial perspective on authigenic clay mineral production in ancient martian lakes. Clays and Clay Minerals, 59, 339–358.

Bristow, T.F., Kennedy, M.J., Morrison, K.M., and Mrofka, D. (2012) The influence of authigenic clay formation on the mineralogy and stable isotopic record of lacustrine carbonates. Geochimica et Cosmochimica Acta, 90, 64–82.

Brown, G., and Brindley, G.W. (1980) X-ray diffraction procedures for clay mineral identification. In G. Brown and G.W. Brindley, Eds., Crystal Structures of Clay Minerals and X-ray Identification. Mineralogical Society Monograph, 5, 305–360.

Campbell, J.L., Perrett, G.M., Gellert, R., Andrushenko, S.M., Boyd, N.I., Maxwell, J.A., King, P.L., and Schofield, C.D.M. (2012) Calibration of the Mars Science Laboratory alpha particle X-ray spectrometer. Space Science Reviews, 170, 319–340.

Chang, H.K., Mackenzie, F.T., and Schoonmaker, J. (1986) Comparisons between the diagenesis of dioctahedral and trioctahedral smectite, Brazilian offshore basins. Clays and Clay Minerals, 34, 407–423.

Changela, H.G., and Bridges, J.C. (2010) Alteration sssemblages in the nakhlites: Variation with depth on Mars. Meteoritics and Planetary Sciences, 45, 1847–1867.

Chipera, S.J., and Bish, D.L. (2002) FULLPAT: A full-pattern quantitative analysis program for X-ray powder diffraction using measured and calculated patterns. Journal of Applied Crystallography, 35, 744–749.

Cornen, G., Bande, G., Giresse, P., and Maley, J. (1992) The nature and chronostratigraphy of Quaternary pyroclastic accumulations from Lake Barombi Mbo (West-Cameroon). Journal of Volcanology and Geothermal Research, 51, 357–374.

Croal, L.R., Johnson, C.M., Beard, B.L., and Newman, D.K. (2004) Iron isotope fractionation by Fe(II)-oxidizing photoautotrophic bacteria. Geochimica et Cosmochimica Acta, 68, 1227–1242.

Cuadros, J., Michalski, J.R., Dekov, V., Bishop, J., Fiore, S., and Dyar, M.D. (2013) Crystal-chemistry of interstratified Mg/Fe-clay minerals from seafloor hydrothermal sites. Chemical Geology, 360-361, 142–158.

Deocampo, D.M., Cuadros, J., Wing-Dudek, T., Olives, J., and Amouric, M. (2009) Saline lake diagenesis as revealed by coupled mineralogy and geochemistry of multiple ultrafine clay phases: Pliocene Olduvai Gorge, Tanzania. American Journal of Science, 309, 834–868.

Derkowski, A., Bristow, T.F., Wampler, J.M., Środoń, J., Marynowski, L., Elliott, W.C., and Chamberlain, C.P. (2013) Hydrothermal alteration of the Ediacaran Doushantuo Formation in the Yangtze Gorges area (South China). Geochimica et Cosmochimica Acta, 107, 279–298.

Dickinson, K.A. (1988) Paleolimnology of Lake Tubutulik, an iron meromictic Eocene Lake, eastern Seward Peninsula, Alaska. Sedimentary Geology, 54, 303–320.

Edwards, K.J., Bach, W., McCollom, T.M., and Rogers, D.R. (2004) Neutrophilic iron-oxidizing bacteria in the ocean: their habitats, diversity, and roles in mineral deposition, rock alteration, and biomass production in the deep-sea. Geomicrobiology Journal, 21, 393–404.

Ehlmann, B.L., and Buz, J. (2015) Mineralogy and fluvial history of the watersheds of Gale, Knobel, and Sharp craters: A regional context for Mars Science Laboratory Curiosity's exploration. Geophysical Research Letters, in press, http://dx.doi.org/10.1002/2014GL062553.

Ehlmann, B.L., Mustard, J.F., Murchie, S.L., Bibring, J-P, Meunier, A., Fraeman, A.A., and Langevin. Y. (2011) Subsurface water and clay mineral formation during the early history of Mars. Nature, 479, 53–60.

Emerson, D., Fleming, E.J., and McBeth, J.M. (2010) Iron-oxidizing bacteria: An environmental and genomic perspective. Annual Review of Microbiology, 64, 561–583.

Evans, B.W., Hattori, K., and Baronnet, A. (2013) Serpentinite: what, why, where? Elements, 9, 99–106.

Farley, K.A., Malespin, C., Mahaffy, P., Grotzinger, J.P., Vasconcelos, P., Milliken, R.E., Malin, M., Edgett, K.S., Pavlov, A.A., Hurowitz, J.A., and others. (2014) In situ radiometric and exposure age dating of the Martian surface. Science, 343, 1247166, http://dx.doi.org/10.1126/science.1247166.

Ferrage, E., Lanson, B., Sakharov, B.A., and Drits, V.A. (2005) Investigation of smectite hydration properties by modeling of X-ray diffraction profiles. Part 1. Montmorillonite hydration properties. American Mineralogist, 90, 1358–1374.

Fordham, A.W. (1990) Formation of trioctahedral illite from biotite in a soil profile over granite gneiss. Clays and Clay Minerals, 38, 179–186.

Galán, E. (2006) Genesis of clay minerals. In F. Bergaya, B.K.G. Theng, and G. Lagaly, Eds., Handbook of Clay Science. Developments in Clay Science, 1, 1129–1162. Elsevier, Amsterdam.

Garcia-Romero, E., Vegas, J., Baldonedo, J.L., and Marfil, R. (2005) Clay Minerals as Alteration Products in Basaltic Volcaniclastic Deposits of La Palma (Canary Islands, Spain). Sedimentary Geology, 174, 237–253.

Gellert, R., Reider, R., Bruekner, J., Clark, B.C., Dreibus, G., Klingelhoefer, G., Lugmair, G., Ming, D.W., Wanke, H., Yen, A., Zipfel, J., and Squyres, S. W. (2006) Alpha particle X-ray spectrometer (APXS): Results from Gusev crater and calibration report. Journal of Geophysical Research, 111, E02S05.

Grotzinger, J.P., Sumner, D.Y., Kah, L.C., Stack, K., Gupta, S., Edgar, L., Rubin, D., Lewis, K., Schieber, J., Mangold, N., and others. (2014) A habitable fluvio-lacustrine environment at Yellowknife Bay, Gale crater, Mars. Science, 343, 1242777, http://dx.doi.org/10.1126/science.1242777.

Hagerty, J.J., and Newsom, H.E. (2003) Hydrothermal alteration at the Lonar Lake impact structure, India: implications for impact cratering on Mars. Meteoritics and Planetary Science, 38, 365–381.

Hahn, B.C., McSween, H.Y., and Tosca, N.J. (2011) Constraints on the stabilities of observed martian secondary mineral phases from geothermal gradient models. Lunar and Planetary Science Conference, 42, abstract 2340.

Hausrath, E.M., and Brantley, S.L. (2010) Basalt and olivine dissolution under cold, salty, and acidic conditions: What can we learn about recent aqueous weathering on Mars? Journal of Geophysical Research, 115, E12001.

Hausrath, E.M., Navarre-Sitchler, A.K., Sak, P.B., Steefel, C.I., and Brantley, S.L. (2008) Basalt weathering rates on Earth and the duration of liquid water on the plains of Gusev Crater, Mars. Geology, 36, 67–70.

Heuser, M., Andrieux, P., Petit, S., and Stanjek, H. (2013) Iron-bearing smectites: a revised relationship between structural Fe, b cell edge lengths and refractive indices. Clay Minerals, 48, 97–103.

Hicks, L.J., Bridges, J.C., and Gurman, S.J. (2014) Ferric saponite and serpentine in the Nakhlite martian meteorites. Geochimica et Cosmochimica Acta, 136, 194–210.

Hover, V.C., and Ashley, G.M. (2003) Geochemical signatures of paleodepositional and diagenetic environments: A STEM/AEM study of authigenic clay minerals from an arid rift basin, Olduvai Gorge, Tanzania. Clays and Clay Minerals, 51, 231–251.

Hurowitz, J.A., Fischer,W.W., Tosca, N.J., and Milliken, R.E. (2010) Origin of acidic surface waters and the evolution of atmospheric chemistry on early Mars. Nature Geoscience, 3, 323–326.

Jones, B.F., and Spencer, R.J. (1999) Clay mineral diagenesis at Great Salt Lake, Utah, USA. Reykjavik, 5th International Symposium on the Geochemistry of the Earth's Surface, 293–297.

Jones, B.F., and Weir, A.H. (1983) Clay minerals of Lake Abert, an alkaline, saline lake. Clays and Clay Minerals, 31, 161–172.

Keller, L.P., Thomas, K.L., Clayton, R.N., Mayeda, T.K. DeHart, J.M., and McKay, D.S. (1994) Aqueous alteration of the Bali CV3 chondrite: Evidence from mineralogy, mineral chemistry, and oxygen isotope compositions. Geochimica et Cosmochimica Acta, 58, 5589–5598.

Klein, F., Bach, W., and McCollom, T.M. (2013) Compositional controls on hydrogen generation during serpentinization of ultramafic rocks. Lithos, 178, 55–69.

Larsen, D. (2008) Revisiting silicate authigenesis in the Pliocene-Pleistocene Lake Tecopa beds, southeastern California: Depositional and hydrological controls. Geosphere, 4, 612–639.

Léveillé, R.J., Bridges, J., Wiens, R.C., Mangold, N., Cousin, A., Lanza, N., Forni, O., Ollila, A., Grotzinger, J.P., Clegg, S., and others. (2014) Chemistry of fracture-filling raised ridges in Yellowknife Bay, Gale crater: Window into past aqueous activity and habitability on Mars. Journal of Geophysical Research: Planets, 119, 2398–2415, http://dx.doi.org/10.1002/2014JE004620.

Lovley, D.R., Giovannoni, S.J., White, D.C., Champine, J.E., Phillips, E., Gorby, Y.A., and Goodwin, S. (1993) *Geobacter metallireducens* gen. nov. sp. nov., a microorganism capable of coupling the complete oxidation of organic compounds to the reduction of iron and other metals. Archives of Microbiology, 159, 336–344.

Lynn, W.C., and Whittig, L.D. (1966) Alternation and formation of clay minerals during cat clay formation. Clays and Clay Minerals, 14, 241–248.

Mahaffy, P.R., Webster, C.R., Cabane, M., Conrad, P.G., Coll, P., Atreya, S.K., Arvey, R., Barciniak, M., Benna, M., Bleacher, L., and others. (2012) The sample analysis at Mars investigation and instrument suite. Space Science Reviews, 170, 401–478.

Maher, B.A., and Taylor, R.M. (1988) Formation of ultrafine-grained magnetite in soils. Nature, 336, 368–370.

Malin, M.C., and Edgett, K.S. (2000) Sedimentary rocks of early Mars. Science, 290, 1927–1937.

Mayhew, L.E., Ellison, E.T., McCollom, T.M., Trainor, T.P., and Templeton, A.S. (2013) Hydrogen generation from low-temperature water-rock reactions. Nature Geoscience, 6, 478–484.

McAdam, A.C., Mahaffy, P.R., Ming, D.W., Brunner, A.E., Archer, D.P., Stern, J.C., Webster, C.R., Graham, H.V., Franz, H.B., Sutter, B., and others. (2014) Analysis of H_2O evolved during pyrolysis of clay-mineral bearing rocks on Mars. 51st Annual Meeting of Clay Minerals Society.

McCollom, T.M., and Bach, W. (2009) Thermodynamic constraints on hydrogen generation during serpentinization of ultramafic rocks. Geochimica et Cosmochimica Acta, 73, 856–875.

McLennan, S.M., Anderson, R.B., Bell, J.F. III, Bridges, J.C., Calef, F. III, Campbell, J.L., Clark, B.C., Clegg, S., Conrad, P., Cousin, A., and others. (2014) Elemental geochemistry of sedimentary rocks at Yellowknife Bay, Gale crater, Mars. Science, 343, 1244734, http://dx.doi.org/10.1126/science.1244734.

Meunier, A. (2005) Clays. Springer, Berlin.

Milliken, R.E., and Bish, D. (2010) Sources and sinks of clay minerals on Mars. Philosophical Magazine, 90, 2293–2308.

Milliken, R.E., Grotzinger, J.P., and Thomson, B.J. (2010) Paleoclimate of Mars as captured by the stratigraphic record in Gale crater. Geophysical Research Letters, 37, L04201.

Ming, D.W., Archer, P.D. Jr., Glavin, D.P. Eigenbrode, J.L., Franz, H.B., Sutter, B., Brunner, A.E., Stern, J.C., Freissinet, C., McAdam, A.C., and others. (2014) Volatile and organic compositions of sedimentary rocks in Yellowknife Bay, Gale crater, Mars. Science, 343, 1245267, http://dx.doi.org/10.1126/science.1245267.

Moore D.M., and Reynolds R.C. (1997) X-ray Diffraction and the Identification and Analysis of Clay Minerals, 378 pp. Oxford Press, New York.

Morris, R.V., Morris, R.V., Ming, D.W., Blake, D.F., Vaniman, D.T., Bish, D.L., Chipera, S.J., Downs, R.T., Treiman, A.H., Yen, A.S., Achilles, C.N., and others. (2013) The amorphous component in martian basaltic soil in global perspective from MSL and MER missions. Lunar and Planetary Science Conference, 44, abstract 1653.

Murchie, S.L., Mustard, J.F., Ehlmann, B.L., Milliken, R.E., Bishop, J.L., McKeown, N.K., Noe Dobrea, E.Z., Seelos, F.P., Buczkowski, D.L., Wiseman, S.M., and others. (2009) A synthesis of Martian aqueous mineralogy after 1 Mars year of observations from the Mars Reconnaissance Orbiter. Journal of Geophysical Research, 114, E00D06.

Neubeck, A., Duc, N.T., Bastviken, D., Crill, P., and Holm, N.G. (2011) Formation of H_2 and CH_4 weathering of olivine at temperatures between 30 and 70°C. Geochemical Transactions, 12, 6.

Olsen, A.A., and Rimstidt, J.D. (2007) Using a mineral lifetime diagram to evaluate the persistence of olivine on Mars. American Mineralogist, 92, 598–602.

Pevear, D.R., Dethier, D.P., and Frank, D. (1982) Clay minerals in the 1980 deposits from Mount St. Helens. Clays and Clay Minerals, 30, 241–252.

Popa, P., Smith, A.R., Popa, R., Jane Boone, J., and Fisk, M. (2012) Olivine-respiring bacteria isolated from the rock-ice interface in a lava-tube cave, a Mars analog environment. Astrobiology, 12, 9–18.

Poulet, F., Bibring, J.-P., Mustard, J.F., Gendrin, A., Mangold, N., Langevin, Y., Arvidson, R.E., Gondet, B., Gomez, C., and the OMEGA Team. (2005) Phyllosilicates on Mars and implications for early martian climate. Nature, 438, 623–627.

Rich, C.I. (1968) Hydroxy interlayers in expansible layer silicates. Clays and Clay Minerals, 16, 15–30.

Rogers, A.D., and Bandfield, J.L. (2009) Mineralogical characterization of Mars Science Laboratory candidate landing sites from THEMIS and TES data. Icarus, 203, 437–453, http://dx.doi.org/10.1016/j.icarus.2009.04.020.

Rogers, A.D., and Christensen, P.R. (2007) Surface mineralogy of martian low-albedo regions from MGS TES data: Implications for crustal evolution and surface alteration. Journal of Geophysical Research, 112, E01003.

Sarrazin, P., Blake, D., Vaniman, D., Chipera, S., and Bish, D. (2005) Field deployment of a portable XRD/XRF instrument on Mars analog terrain. Powder Diffraction, 20, 128–133.

Sato, T., Watanabe, T., and Otsuka, R. (1992) Effects of layer charge, charge location, and energy change on expansion properties of dioctahedral smectites. Clays and Clay Minerals, 40, 103–113.

Schwenzer, S.P., Abramov, O., Allen, C.C., Clifford, S., Filiberto, J., Kring, D.A., Lasue, J., McGovern, P.J., Newsom, H.E., Treiman, A.H., and Wittmann, A. (2012) Gale crater: Impact processes, impact-generated hydrothermal activity and potential habitats for life. Planetary and Space Science, 70, 84–95, http://dx.doi.org/10.1016/j.pss.2012.05.014.

Siebach, K.L., Grotzinger, J.P., Kah, L.C., Stack, K.M., Malin, M., Léveillé, R., and Sumner D.Y. (2014) Subaqueous shrinkage cracks in the Sheepbed Mudstone: Implications for early fluid diagenesis, Gale crater, Mars. Journal of Geophysical Research: Planets, 119, 1597–1613, http://dx.doi.org/10.1002/2014JE004623.

Stack, K.M., Grotzinger, J.P., Kah, L.C., Schmidt, M.E., Mangold, N., Edgett, K.S., Siebach, K.L., Nachon, M., Lee, R., Blaney, D.L., and others. (2014) Diagenetic origin of nodules and hollow nodules of the Sheepbed Member, Yellowknife Bay formation, Gale crater, Mars. Journal of Geophysical Research: Planets 119, 1637–1664, http://dx.doi.org/10.1002/2014JE004617.

Stevens, T.O., and McKinley, J.P. (2000) Abiotic controls on H_2 production from basalt-water reactions and implications for aquifer biogeochemistry. Environmental Science and Technology, 34, 826–831.

Stopar, J.D., Taylor, G.J., Hamilton, V.E., and Browning, L. (2006) Kinetic model of olivine dissolution and extent of aqueous alteration on Mars. Geochimica et Cosmochimica Acta, 70, 6136–6152.

Straub, K.L., and Buchholz-Cleven, B.E. (1998) Enumeration and detection of

anaerobic ferrous iron-oxidizing, nitrate-reducing bacteria from diverse European sediments. Applied and Environmental Microbiology, 64, 4846–4856.
Suquet, H., and Pezerat, H. (1987) Parameters influencing layer stacking in saponite and vermiculite: A review. Clays and Clay Minerals, 35, 353–362.
Suquet, H., de la Calle, C., and Pezerat, H. (1975) Swelling and structural organization of saponite. Clays and Clay Minerals, 23, 1–9.
Taylor, R.M., Maher, B.A., and Self, P.G. (1987) Magnetite in soils. I. The synthesis of superparamagnetic and single domain magnetite. Clay Minerals, 22, 411–422.
Tomeoka, K., and Buseck, P.R. (1990) Phyllosilicates in the Mokoia CV carbonaceous chondrite: Evidence for aqueous alteration in an oxidizing condition. Geochimica et Cosmochimica Acta, 54, 1787–1796.
Tosca, N.J., and Knoll, A.H. (2009) Juvenile chemical sediments and the long term persistence of water at the surface of Mars. Earth and Planetary Science Letters, 286, 379–386.
Treiman, A.H., Barrett, R.A., and Gooding, J.L. (1993) Preterrestrial aqueous alteration of the Lafayette (SNC) meteorite. Meteoritics, 28, 86–97.
Treiman, A.H., Morris, R.V., Agresti, D.G., Graff, T.G., Achilles, C.N., Rampe, E.B., Bristow, T.F., Ming, D.W., Blake, D.F., Vaniman, D.T., and others. (2015) Ferrian saponite from the Santa Monica Mountains (California, USA, Earth): Characterization as an analog for clay minerals on Mars with application to Yellowknife Bay in Gale crater. American Mineralogist, 99, 2234–2250.
Ufer, K., Roth, G., Kleeberg, R., Stanjek, H., Dohrmann, R., and Bergmann, J. (2004) Description of X-ray powder pattern of turbostratically disordered layer structures with a Rietveld compatible approach. Zeitschrift fur Kristallographie Supplements, 219, 519–527.
Vaniman, D.T., Bish, D.L., Ming, D.W., Bristow, T.F., Morris, R.V., Blake, D.F., Chipera, S.J., Morrison, S.M., Treiman, A.H., Rampe, E.B., and others. (2014) Mineralogy of a mudstone at Yellowknife Bay, Gale crater, Mars. Science, 343, 1243480, http://dx.doi.org/10.1126/science.1243480.
Weaver, C.E. (1989) Clays, Muds, and Shales. Elsevier, Amsterdam.
Weiss, J.V., Emerson, D., Backer, S.M., and Megonigal, J.P. (2003) Enumeration of Fe(II)-oxidizing and Fe(III)-reducing bacteria in the root zone of wetland plants: implications for a rhizosphere iron cycle. Biogeochemistry, 64, 77–96.
Widdel, F., Schnell, S., Heising, S., Ehrenreich, A., Assmus, B., and Schink, B. (1993) Ferrous iron oxidation by anoxygenic phototrophic bacteria. Nature, 362, 834–836.
Wiens, R.C., Maurice, S., Barraclough, B., Saccoccio, M., Barkley, W.C., Bell, J.F. III, Bender, S., Bernardin, J., Blaney, D., Blank, J., and others. (2012) The ChemCam instrument suite on the Mars Science Laboratory (MSL) rover: Body unit and combined system performance. Space Science Reviews, 170, 167–227.
Wilson, J., Cuadros, J., and Cressey, G. (2004) An in situ time-resolved XRD–PSD investigation into Na-montmorillonite interlayer and particle rearrangement during dehydration. Clays and Clay Minerals, 52, 180–191.
Wilson, J., Savage, D., Cuadros, J., Shibata, M., and Ragnarsdottir, K.V. (2006) The effect of iron on montmorillonite stability: I. Background and thermodynamic considerations. Geochimica et Cosmochimica Acta, 70, 306–322.
Wray, J.J. (2013) Gale crater: the Mars Science Laboratory/Curiosity Rover landing site. International Journal of Astrobiology, 12, 25–38.
Ziegler, K., Hsieh, J.C.C., Chadwick, O.A., Kelly, E.F., Hendricks, D.M., and Savin, S.M. (2003) Halloysite as a kinetically controlled end product of arid-zone basalt weathering. Chemical Geology, 202, 469–486.

Manuscript received June 4, 2014
Manuscript accepted September 20, 2014
Manuscript handled by Janice Bishop